Wave-Particle Interactions in Electron Acoustic Waves in Pure Ion Plasmas

F. Anderegg, C. F. Driscoll, D. H. E. Dubin, and T. M. O'Neil

Department of Physics, University of California at San Diego, La Jolla, California 92093, USA
(Received 23 September 2008; published 2 March 2009)

Electron acoustic waves (EAW) with a phase velocity less than twice the plasma thermal velocity are observed on pure ion plasma columns. At low excitation amplitudes, the EAW frequencies agree with theory, but at moderate excitation the EAW is more frequency variable than typical Langmuir waves, and at large excitations resonance is observed over a broad range. Laser induced fluorescence measurements of the wave-coherent ion velocity distribution show phase reversals and wave-particle trapping plateaus at $\pm v_{\text{ph}}$, as expected, and corroborate the unusual role of kinetic pressure in the EAW.

Electron acoustic waves (EAW) are electrostatic plasma waves with an unusually small phase velocity compared to Langmuir waves. They have been extensively studied theoretically [1,2] and numerically [3], generally in the weakly nonlinear limit where a small flattening of the particle distribution at v_{ph} eliminates the otherwise strong Landau damping. Simulations, theory, and pure electron plasma experiments [4] corroborated the low frequencies predicted for small-amplitude EAWs. Recently, EAW modes have been identified as contributing to back-scatter light in laser-foil experiments [5,6], and simulations [7,8] and analysis [9] of electromagnetic-electrostatic mode couplings in these bounded, relativistic plasmas support the EAW interpretation. Simpler Vlasov-Poisson simulations [10] have probed the highly nonlinear amplitude regime, suggesting that EAW-like modes with strong harmonic content (called KEEN waves) can be excited over a wide range of frequencies.

In this Letter we characterize misleadingly named EAW frequencies and wave-particle interactions in trapped pure ion plasma columns, in the small- and large-amplitude regimes. The ion plasma EAWs are directly analogous to EAWs in neutral plasmas or pure electron plasmas, since only one species participates in the wave. The measurements verify the dispersion relation predicted for small-amplitude EAWs, and demonstrate the strong frequency variability of large-amplitude waves. The LIF measurements directly image the velocity-space trapping, and elucidate the unusual negative dynamical compressibility which produces the low EAW frequencies.

The ion plasma trap consists of a series of hollow conducting cylinders of radius $R_w = 2.86$ cm contained in ultrahigh vacuum at $P \approx 10^{-10}$ Torr, with a uniform axial magnetic field of $B = 3$ T. The plasma is singly-ionized magnesium (79% ^{24}Mg$^+$, 10% ^{25}Mg$^+$, 11% ^{26}Mg$^+$), with total density is $n \sim 1.5 \times 10^7$ cm^{-3}, over a radius $R_p \sim 0.45$ cm, with length $L_p \simeq 9$ cm centered around $z = 0$. The quiescent plasma has a Maxwellian velocity distribution, with temperature controlled over the range $0.3 < T < 1.5$ eV. These parameters give Debye length $0.1 < \lambda_D <$

0.24 cm, thermal velocities $110. < \bar{v} \equiv \sqrt{T/m} < 245.$ cm/ms, ion-ion collision rates $8 > \nu_{ii} > 0.7\text{sec}^{-1}$, and plasma frequency $f_p = 165$ kHz. The plasma is held in steady state with a weak "rotating wall" electric field [11], which is turned off for the 200 ms of each wave measurement.

We excite standing EAWs and higher-frequency Langmuir waves (denoted Trivelpiece-Gould waves in bounded cylindrical geometry). Both waves are azimuthally symmetric ($m_\theta = 0$), with longest possible axial wavelength ($m_z = 1$) $\lambda \approx 2L_p$, and with lowest radial mode numbers ($m_r = 1$). The waves are excited by an amplitude-rounded burst of ~ 100 cycles at chosen frequency f_{exc} and amplitude A_{exc}, applied to a cylinder of z-extent $(2.9 \rightarrow 8.7 \text{ cm})$. The subsequent wave-induced wall voltage $V_w(t)$ is recorded from a separate cylinder of z extent $(-2.9 \rightarrow 0 \text{ cm})$, and is fit in overlapping time segments as

$$V_w(t) = A_w(t)\cos(\theta_w(t)) \qquad (1)$$

giving $\theta_w(t)$, with slowly damping $A_w(t)$ and $f_w(t) \equiv d\theta_w/2\pi dt$.

When the amplitude is turned down sufficiently ($A_{\text{exc}} \sim 50$ mV), the waves are observed only at their resonant frequencies, plotted in Fig. 1 as dots (EAW) and squares (TG wave) for different temperatures. These dots agree well with the near-linear theory $f_{\text{EAW}}(T)$ of Refs. [1,3]. At temperatures above 1.3 eV no waves are observed at comparably low excitation amplitude. The EAWs are observed to damp exponentially at these small amplitudes, with $30 < \gamma < 3000$ s^{-1}; and this is about 10× faster than TG waves in this regime. However, at larger amplitude, the waves are excited over a range of different frequencies and furthermore they ring at frequencies different than f_{EAW} or f_{exc} because the excitation has significantly modified the distribution function. Excitation of EAW modes requires about 10× greater amplitude and/or duration compared to TG waves. With insufficient excitation, the EAW damps within a few cycles, because the requisite distribution flattening near v_{ph} has not been effected.
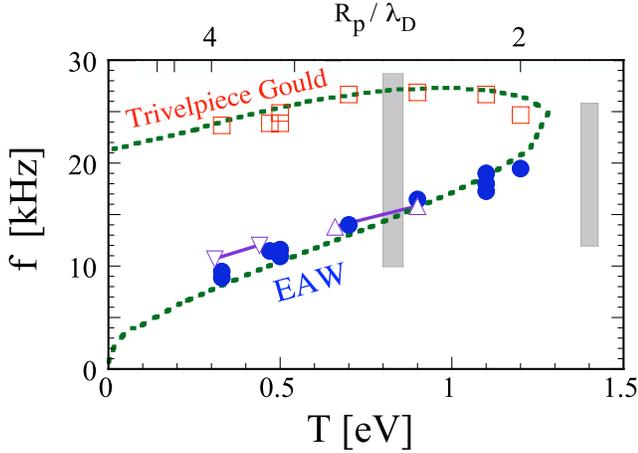
FIG. 1 (color online).   Measured small-amplitude wave dispersion and theory (dashed) for EAW and TG modes. Stronger drive gives any frequency waves (gray bars).

The predicted EAW and Langmuir dispersion would be a distinctive "thumb" shape [1] for unbounded plasmas, with the fast Langmuir $f(k_z)$ rising gently from f_p, and the slow acoustic EAW $f(k_z)$ meeting it at $k_{tot}\lambda_D \sim \frac{1}{2}$. In these radially bounded plasmas, the fast (TG) branch is also acoustic [12], with frequency $f_{TG} = f_p k_z / k_{tot}$ plus thermal corrections, with $k_{tot}^2 \equiv k_z^2 + k_\perp^2$, $k_\perp \equiv x_r/R_p$, and $x_r^2 \approx 2/\ln(R_w/R_p) \sim 1.4$. The predicted EAW dispersion [3] is always acoustic, with $f_{EAW} = \alpha \bar{v} k_z/2\pi$; for unbounded plasmas theory predicts normalized phase velocity $\alpha \equiv v_{ph}/\bar{v} \equiv 2\pi f/k_z \bar{v} \sim 1.3$, and for our bounded plasmas we find $1.4 < \alpha < 2.1$. The theory curve (dashed) of Fig. 1 is obtained from the prescription of Ref. [3], giving $\alpha = 1.7$ at $T = 0.7$ eV.

However, we find that EAW-like modes can be readily excited over a range of frequencies around the small-amplitude resonant frequencies, using only "moderate" amplitude drives. An off-resonant drive at f_{exc} readily modifies the velocity distribution $F(v)$ so as to make the mode resonant, continuing to ring at $f_w = f_{exc}$; and this occurs for f_{exc} above *or* below the near-linear f_{EAW}. Adjustment to resonance for $f_{exc} > f_{EAW}$ could be explained by simple heating; but adjustment to resonance for $f_{exc} < f_{EAW}$ requires a more subtle rearrangement of $F(v)$. The bar at $T = 0.8$ eV in Fig. 1 represents the range of frequencies over which a 100 cycle burst with $A_{exc} = 300$ mV resulted in a wave with $f_w = f_{exc}$ continuing for hundreds to thousands of cycles, i.e., with $\gamma/f \lesssim 10^{-2}$. Similarly, EAW-like waves can be excited at high temperatures where no near-linear solution exists: $A_{exc} = 200$ mV for 100 cycles on a $T = 1.4$ eV plasma resulted in robust modes in the band of frequencies shown in Fig. 1.

The distinctive features of these EAW-like modes arise because v_{ph} lies in the body of the velocity distribution $F_0(v)$. For a *single* travelling wave with potential $\delta\phi_1(z,t) = A_1 \exp\{ik_z(z - v_{ph}t)\}$, linear theory predicts velocity perturbations from the wave potential, as

$$\delta F_1(v) = (q\delta\phi_1/m)\frac{\partial F_0/\partial v}{v - v_{ph}}. \quad (2)$$

The density perturbation from particles moving faster than v_{ph} partially cancels the (opposite-sign) density perturbation from the slower bulk particles; and the negative pressure from particles with $v > v_{ph}$ will be seen to be dominant.

Here, we measure $\delta F(v)$ for a *standing* EAW by performing laser induced fluorescence doppler spectroscopy correlated with the phase θ_w of the received wave similar to Fig. 4 of Ref. [13]. The plasma near radial center is illuminated with a laser beam resonant with ions having z velocity v_ℓ, and individual fluorescent photons received at $z = 0$ are detected, giving a "rate" $P(v_\ell, t)$ at which photons are detected, represented by a series of delta-functions. The correlation integral

$$\delta F(v_\ell) \equiv \int_{t_1}^{t_2} dt \frac{P(v_\ell, t)}{t_2 - t_1} \cos[(\theta_w(t) - \theta_w(0)] \quad (3)$$

is then calculated, with (t_1, t_2) encompassing $\sim 10^3$ photons over ~ 100 wave cycles after excitation. Repeating this process for 250 velocities v_ℓ (on the same plasma, each after 5 sec of reequilibration) then gives $\delta F(v)$, here in units of photons/ms for 1 mW of illumination.

Figure 2(a) displays the coherent $\delta F(v)$ (dots) for a standing EAW excited to moderate amplitude at $f = 10.7$ kHz ($\triangledown$ in Fig. 1), compared to the prediction (curve) from a "two wave-trapping" model described below. The sign-change at $v = 0$ comes from $\partial F_0/\partial v$, and sign changes are observed at $v_{ph} = \pm 208$ cm/ms from the two counterpropagating waves, as expected from Eq. (2). The measured v_{ph} gives wavelength $\frac{1}{2}\lambda = v_{ph}/2f = 9.7$ cm, i.e., about 10% larger than L_p, as is typical of waves in these traps [14].

A similar wave-coherent LIF technique gives the full ion velocity distribution $F(v, \theta_j)$ for each of 8 wave phase-bins $\theta_j = 2\pi(j/8)$, again only at $z = 0$. Figure 2(b) shows 5 of these 8 phase bins, plus the phase-averaged distribution $\langle F(v) \rangle$ before, during, and after the wave. Before the wave, $\langle F \rangle$ closely matches a Maxwellian with $T = 0.31$ eV; during the initial 10 ms of the wave, $\langle F \rangle$ shows a bulge which is flat only locally at $\pm v_{ph}$; and 100 ms after excitation, the wave has damped and $\langle F \rangle$ is a barely distorted Maxwellian approximated by $T = 0.44$ eV. (The persistent glitches just to the left of $v = 0$ and the 10% left-right sensitivity differences are laser-cooling artifacts.) In contrast, the phase-coherent $F(v, \theta_j)$ curves show the two broadly flattened trapping regions around $\pm v_{ph}$, of maximal extent for phases $j = 1$ and $j = 5$. These wave-trapped particles propagate in the wave troughs past the photon detector at $z = 0$, and then reflect at the plasma ends, remaining trapped during hundreds of end reflections.

The curves of Fig. 2 represent a simple standing-wave model of phase space, superimposing 2 *phase-locked*
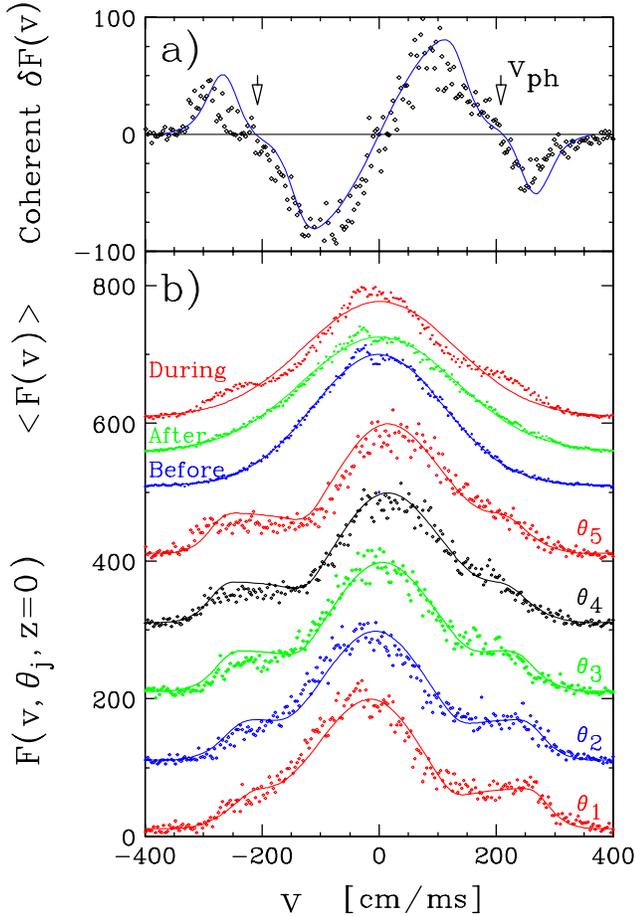
FIG. 2 (color online). (a) Measured coherent $\delta F(v)$; (b) Measured phase-binned $F(v, \theta_j)$ for 5 of 8 bins, and average $\langle F(v) \rangle$ before, during and after the wave; all compared to standing-wave model (curves).

waves of amplitude A_1 with opposite v_{ph}, each perturbing and trapping particles in *separate* Maxwellian distributions. The model distributions conserve energy $\varepsilon = \frac{1}{2}mw^2 + q\delta\phi_1(z)$ separately in each wave frame defined by $w \equiv v \pm v_{ph}$. A smooth transition from trapped (t) to untrapped (u) particles is modeled by [15]

$$F_t(\varepsilon) = \exp\{-(qA_1 + \tfrac{1}{2}mv_{ph}^2)/T\} \quad \text{for } \varepsilon < qA_1$$

$$F_u(\varepsilon) = \exp\{-(\varepsilon + \tfrac{1}{2}mv_{ph}^2 \pm v_{ph}u(\varepsilon))/T\} \quad \text{for } \varepsilon > qA_1,$$
$$(4)$$

with $\pm$ representing $w > 0$ and $w < 0$, $u(\varepsilon) \equiv \int_{q\phi_1}^{\varepsilon} d\varepsilon'/I(\varepsilon')$, and $I(\varepsilon) \equiv \int_0^{L_p} (dz/L_p)[2\varepsilon - 2q\phi(z)]^{1/2}$. Finally, the model is smoothed to the spatial and velocity definition of the experiment, with $\delta z/L_p$ and $\delta v/2\bar{v}$ about 1/20. Although simplistic in some details, this model contains the essence of particle trapping and two-wave superposition required to interpret the measurements. For example, Eq. (2) suggests singularities at $\pm v_{ph}$, but this is mitigated by the trapping width Δv_T setting a lower limit

for v-v_{ph}, by the presence of 2 waves, and by the experimental resolution.

In Fig. 3, the EAW data (and modeling) of Fig. 2 are presented as a phase-space-like image of $F(v, \theta_w)$. Two wave characteristics clearly visible in Figs. 2 and 3 are the oscillating shift δv_0 of the distribution peak, and full wave-trapping plateaus widths $2\Delta v_T$. These are quantitatively determined by the photon data. For the standing-wave model, these are predicted to be of magnitude

$$\delta v_0 v_{ph} = 2qA_1/m \qquad (\Delta v_T)^2 = 4qA_1/m. \qquad (5)$$

Figure 4 shows the measured δv_0 and Δv_T during the damping of two separate standing EAWs, parameterized by the received *wall* voltage amplitude A_{w2}. The open symbols ($\diamond$, $\square$) show the wave of Figs. 2 and 3; and the solid symbols show a more strongly excited wave at $f = 13.8$ kHz on a $T = 0.66$ eV plasma. The A_{w2} error bars span the received amplitude during 5 ms time bins, and the trapping width Δv_T is a visual estimate from $F(v, \theta_j)$. The dashed lines represent Eqs. (5), using a wall-voltage to 1-wave potential calibration $A_{w2} = (1.2 \times 10^{-3})2A_1$. The oscillating body velocity δv_0 decreases as $\delta v_0 \propto A_{w2}$ for both waves, as expected.

The trapping width Δv_T of the smaller wave is observed to decrease "immediately" during wave damping, as $\Delta v_T \propto A_{w2}^{1/2}$. Flat wave-frame "cat's-eye" regions in $F(v, z)$ do not imply a flat lab-frame $F(v)$ anywhere except possibly $\pm v_{ph}$, and so no collisions are required to decrease the observed Δv_T. For the largest trapping regions, collisional smoothing would be expected at a rate $\nu_s \sim \nu_{ii}\bar{v}^2/\Delta v_T^2 \sim 16$ sec^{-1}, i.e., in a time comparable to the total evolution of the waves; and smaller regions would be smoothed faster. In contrast, the larger wave develops *nonoscillating* dc plateaus at $\pm v_{ph}$ which persist even after
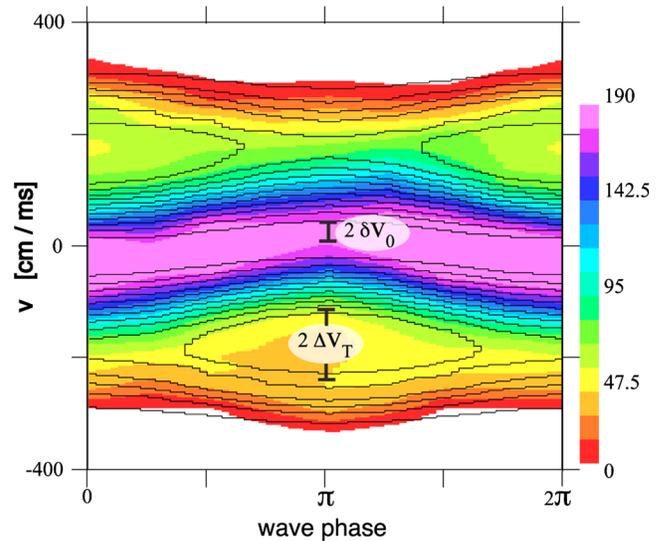

FIG. 3 (color online). Measured phase-space-like $F(v, \theta_w, z = 0)$ image for the EAW of Fig. 2 represented by color contours; the lines represent the standing-wave model.
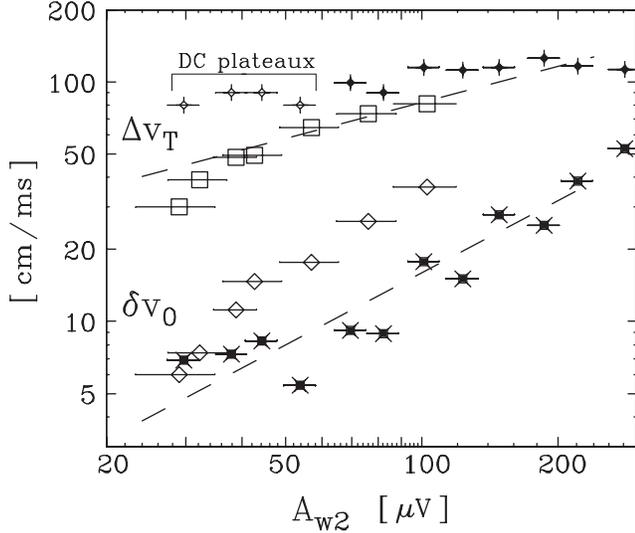
FIG. 4. Measured δv_0 and Δv_T during decay of two EAWs. Dashed lines are prediction of Eqs. (5).

the wave has largely damped. This larger wave exhibits "fully nonlinear" effects of strong phase-locked harmonic content at $2f$ in the received wall signal. These two waves are represented by the △'s and ▽'s of Fig. 1, showing the initial and final plasma temperatures and wave frequencies.

From a fluid perspective, the low frequency of the EAW arises because of an unusual *negative* dynamical compressibility: the pressure oscillations are 180° out of phase from the density oscillations, almost fully canceling the electrostatic restoring force. We consider the oscillating density $\delta n \equiv \int dv \delta F$, fluid velocity $\delta V_f \equiv \int dv v \delta F$, and pressure $\delta P \equiv \int dv (v - V_f)^2 \delta F$. The first two moments of the Vlasov equation give

$$V_f/v_{\rm ph} = \delta n/n,$$

$$\delta V_f v_{\rm ph} = 2(q\delta\phi_1/m + \delta P/nm) \equiv (2q\delta\phi_1/m)(1 + \chi).$$
(6)

Here, χ^{-1} is the scaled dynamical compressibility given by $\chi^{-1} \equiv (\delta n/\delta P)(m\omega_p^2/k_{\rm tot}^2)$, where we have used Poisson's equation $k_{\rm tot}^2 \delta\phi_1 = 4\pi e \delta n$. Combining Poisson's equation with Eqs. (6) gives χ in terms of $(k_z, k_\perp)$ and wave frequency f, and simple low temperature limits can be obtained from kinetic theory, giving

$$\chi = \frac{k_{\rm tot}^2}{k_z^2}\frac{f^2}{f_p^2} - 1 \xrightarrow{\rm TG} 3k_\perp^2 \lambda_D^2$$

$$\xrightarrow{\rm EAW} -1 + \alpha^2 k_\perp^2 \lambda_D^2.$$
(7)

The values of χ obtained from the experimental parameters are consistent with the theory perspective of Eq. (7). For the TG mode at $T = 0.3$ eV with $v_{\rm ph} \gg \bar{v}$, the pressure is small and $\chi \sim 0.29$; the electrostatic restoring force predominantly determines the frequency and $v_{\rm ph}$. For the

corresponding EAW mode, $\chi \sim -0.65$; the negative pressure from $v > v_{\rm ph}$ particles in Eq. (2) almost cancels the electrostatic restoring force, with the small thermal term determining the (low) frequency. From this perspective, it is not surprising that nonlinear effects which modify $\langle F(v)\rangle$ can readily change the frequency of these low-phase-velocity EAWs.

It is worth noting that the mode frequencies observed here are well approximated by the Dorning theoretical approach, even for the large-amplitude case. For example, utilizing one of the measured velocity distributions of Fig. 2(b), one obtains $v_{\rm ph}/\bar{v} = 1.85$ compared to the coherently measured $v_{\rm ph}/\bar{v} = 1.86$ [16]. However, the driver strength, duration, and coupling characteristics determine the initial transients and strongly affect $\langle F\rangle$, so predicting plasma response and mode couplings from the initial $F(v)$ remains difficult.

[1] J. P. Holloway and J. J. Dorning, Phys. Rev. A **44**, 3856 (1991).
[2] H. Schamel, Phys. Plasmas **7**, 4831 (2000).
[3] F. Valentini, T. M. O'Neil, and D. H. E. Dubin, AIP Conf. Proc. No. 862 (AIP, New York, 2006) p. 3
[4] A. A. Kabantsev, F. Valentini, and C. F. Driscoll, in *NNP VI*, edited by M. Drewsen *et al.*, AIP Conf. Proc. No. 862 (AIP, New York, 2006) p. 13; F. Valentini, T. M. O'Neil and D. H. E. Dubin, Phys. Plasmas **13**, 052303 (2006).
[5] D. S. Montgomery *et al.*, Phys. Rev. Lett. **87**, 155001 (2001).
[6] N. J. Sircombe, T. D. Arber, and R. O. Dendy, Plasma Phys. Controlled Fusion **48**, 1141 (2006).
[7] Lj. Nikolić, M. M. Ŝkorić, S. Ishiguro, and T. Sato, Phys. Rev. E **66**, 036404 (2002).
[8] A. Ghizzo, T. W. Johnston, T. Réwéille, P. Bertrand, and M. Albrecht-Marc, Phys. Rev. E **74**, 046407 (2006).
[9] H. A. Rose and D. A. Russell, Phys. Plasmas **8**, 4784 (2001).
[10] B. Afeyan *et al.*, *Proceedings of the Inertial Fusion Sciences and Applications 2003, Monterey*, edited by B. Hamel *et al.* (Am. Nucl. Soc., LaGrange Park, IL, 2004), p. 213.
[11] X.-P. Huang, F. Anderegg, E. M. Hollmann, C. F. Driscoll, and T. M. O'Neil, Phys. Rev. Lett. **78**, 875 (1997).
[12] A. W. Trivelpiece and R. W. Gould, J. Appl. Phys. **30**, 1784 (1959).
[13] F. Skiff and F. Anderegg, Phys. Rev. Lett. **59**, 896 (1987).
[14] J. K. Jennings, R. L. Spencer, and K. C. Hansen, Phys. Plasmas **2**, 2630 (1995).
[15] V. E. Zakharov and V. I. Karpman, JETP **16**, 351 (1963).
[16] F. Valentini (private communication).